CHAPTER 3
MICROSTRUCTURAL CHARACTERIZATION AND MICROHARDNESS OF GRADIENT STRUCTURED AA7075

3.1 Introduction

This chapter illustrates the role of ultrasonic shot peening on microstructural and morphological modifications of the peak aged samples of AA7075. Disk shaped samples were subjected to ultrasonic shot peening for different time intervals with hard steel balls of 3 mm at a constant amplitude of 80 μm. The refinement in the near surface microstructure was examined using transmission electron microscope and X-ray diffraction. The microstructure evolutions of the specimens along the depth from the USSP treated surface were examined by transmission electron microscope (TEM) and electron back scattered diffraction (EBSD) associated with field emission scanning electron microscope (FESEM). The variation of microhardness and residual stress along the section perpendicular to the USSP treated surface from the surface towards the interior was also measured. The samples USSP treated for 15 s, 30 s, 60 s, 180 s and 300 s are designated as USSP 15, USSP 30, USSP 60, USSP 180 and USSP 300, respectively.

3.2 Microstructure Characterization

The microstructure of the peak aged AA7075 aluminium alloy was studied using optical microscope. The optical micrograph in Fig. 3.1 shows dual phase microstructure with Mg-rich precipitates and some intermetallic particles distributed homogeneously in the α-phase matrix.

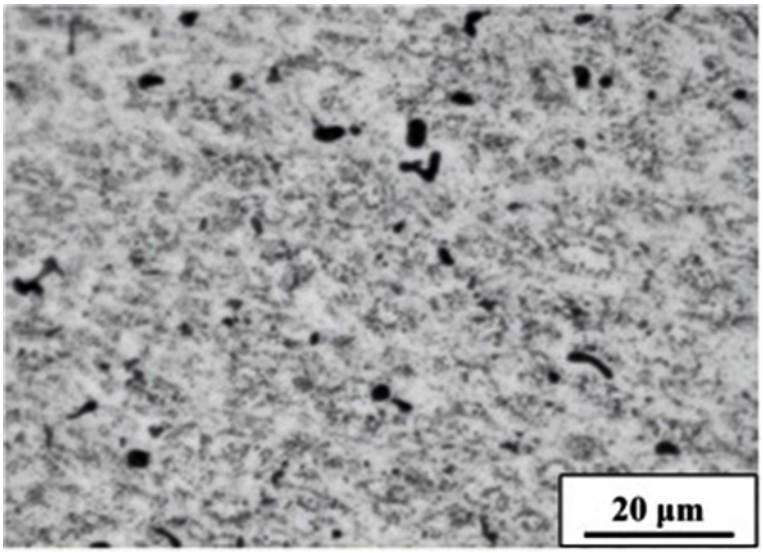

FIGURE 3.1: Optical micrographs showing microstructure of the AA7075 in RRA condition.

3.2.1 Surface topography

Surface topography of the samples USSP treated for different durations are shown in Fig. 3.2. The smoothness of the un-USSP sample is quite evident from Fig. 3.2a whereas there are distinct impressions of the steel balls on the surface of the USSP 15 specimen (Fig. 3.2b). However, with increase in the duration of USSP, the morphology of the surface changed and dark patches appeared showing the depressed regions resulting from erosion of the surface in those regions from longer durations of USSP (Fig. 3.2c, d, e).

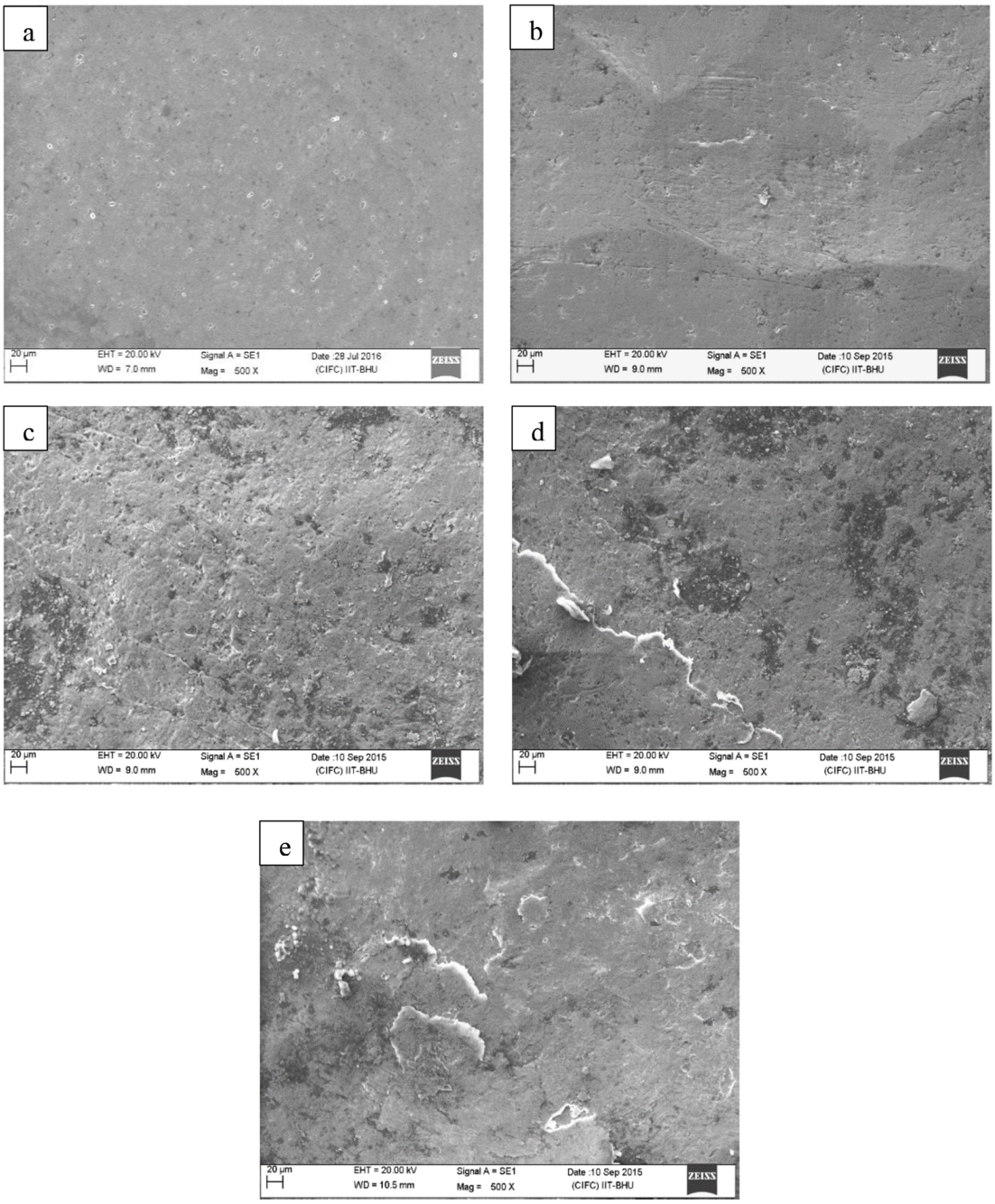

FIGURE 3.2: Surface topography of the AA7075 samples in (a) un-USSP condition & USSP treated respectively for different durations (b) 15 s, (c) 30 s, (d) 60 s, & (e) 300 s.

Also, chipping may be seen on the surface of the USSP 60 specimen (Fig. 3.2d) and there is multi layer chipping on the surface of the USSP 300 sample (Fig. 3.2e).

SEM images of the USSP 15, USSP 60 and USSP 300 samples, sectioned perpendicular to the USSP treated surfaces are shown in Fig. 3.3. It is evident that while the edge of the USSP15 and USSP 60 samples are smooth (Fig. 3.3 a, b) there is flaking and cracking in the case of USSP 300 sample (Fig. 3.3c).

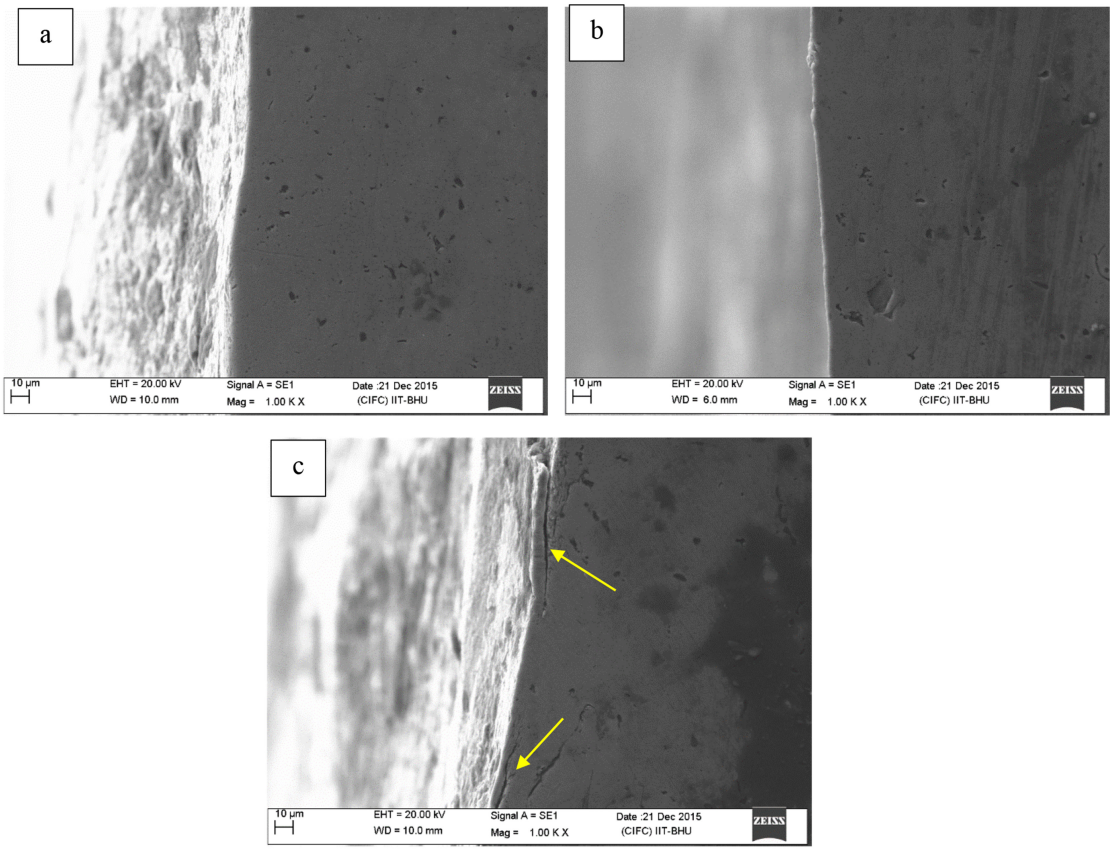

FIGURE 3.3: Cross-Sectional SEM image of the AA 7075 USSP treated for different durations: (a) 15 s, (b) 60 s and (c) 300 s

3.2.2 Characterization of precipitates through TEM

The microstructure in the PA-unUSSP condition consists of very fine Guinier-Preston zones, plate shaped η' precipitates within the grains, equiaxed η ($MgZn_2$) precipitates

segregated mostly at the grain boundaries and some large intermetallic particles of the E-phase ($Al_{18}Cr_2Mg_3$) distributed throughout the microstructure.

Most of the grains were dislocation free and there was very low density of dislocations in some grains. High-resolution transmission electron microscopy (HRTEM) was carried out to characterize the fine structure consisting of GP-zones and η' precipitates shown in Fig. 3.4b & 3.4d.

Fig. 3.4b shows a GP-zone of $\sim$ 5 nm in size and there is no mismatch between the lattice planes of GP-zone and Al matrix suggesting coherency between these phases. The presence of coherent lattice planes is also obvious from the inverse fast fourier transform (IFFT) image (Fig. 3.4c) of the dashed frame in Fig. 3.4b. The HRTEM image in Fig. 3.4d corresponds to η' of an average diameter size of $\sim$ 10 nm. It is evident from the IFFT image (Fig. 3.4e) that there is no perfect coherency between the lattice planes of the precipitate and the Al matrix and also there is presence of dislocations at the interface due to semi-coherent nature of the η' precipitates. GP-zones induce considerable plastic strain into the Al-matrix due to which they appear to be thick at lower magnification, therefore HRTEM was carried out to differentiate GP-zones from η' precipitates. The STEM-HAADF was performed to characterize the coarse precipitates. The precipitate in Fig. 3.4f was found enriched in Mg and Zn suggesting $MgZn_2$, whereas the precipitate in Fig. 3.4g was enriched with Mg and Cr confirming the presence of E-phase.

The stable η-phase was found to be present in two types, one with spherical morphology and considerable disorder (Fig. 3.5a) and the other as ordered structure (Fig. 3.5b)

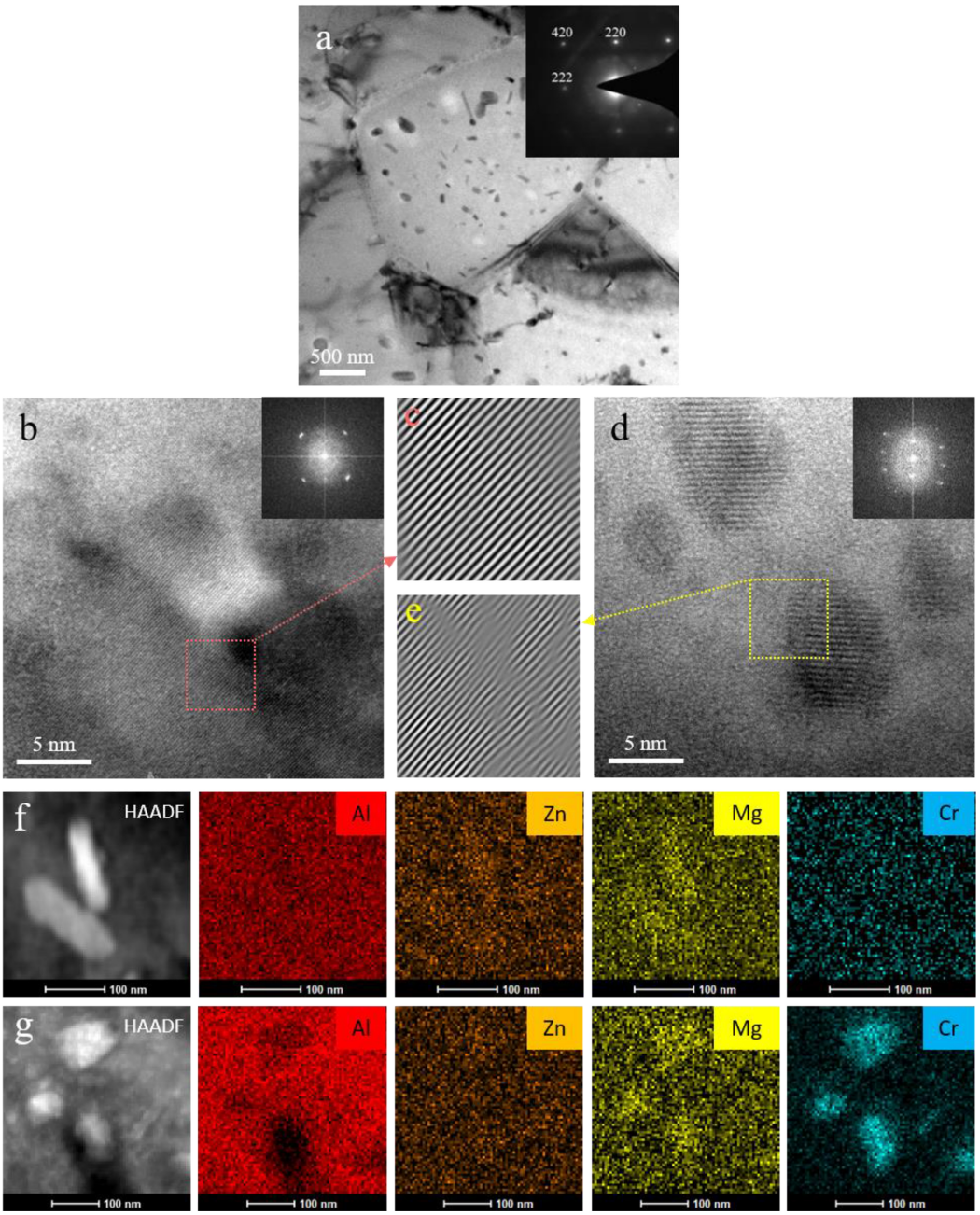

FIGURE 3.4: Bright field TEM micrographs of the AA7075: (a) PA-unUSSP, (b) HRTEM image of GP-zone, (c) corresponding IFFT pattern of framed region in Fig. b, (c) HRTEM image of η' precipitate, (e) corresponding IFFT pattern of framed region in Fig.c, HAADF-STEM image and EDS mapping of Al,Zn, Mg and Cr of (f) η-phase and (g) E-phase respectively.

consisting of a set of parallel line contrasts. The large plate shaped particles were identified as η' precipitates (semi-coherent) and the needle shaped as η-precipitates (incoherent).

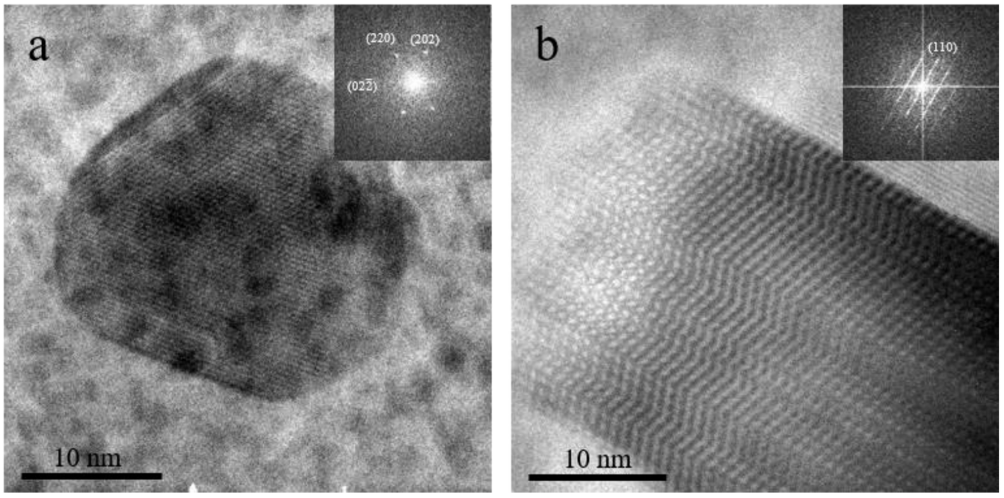

FIGURE 3.5: HRTEM micrographs of η-phase and its corresponding FFT (a) spherical and (b) needle morphology in PA-unUSSP condition

3.2.2.1 Surface microstructure of the USSP treated region

The TEM micrographs and the corresponding selected area electron diffraction (SAED) patterns of the USSP 15, USSP 30, USSP 60, USSP 180 and USSP 300 samples are shown in Fig. 3.6. High strain rate during continuous peening of balls in surface region causes subdivision of the original coarse grains. There was formation of large number of nanograins of 28 nm, 28 nm, 26 nm, 21 nm and 19 nm size in surface regions of the samples USSP treated for 15, 30, 60, 180 and 300 seconds respectively. Nano grain formation was also confirmed from the ring patterns of the SAED resulting from random crystallographic orientations.

With increase in the USSP duration from 15 to 300 seconds there was further refinement of grains. Some precipitates are visible in the USSP 15 sample but not in the USSP

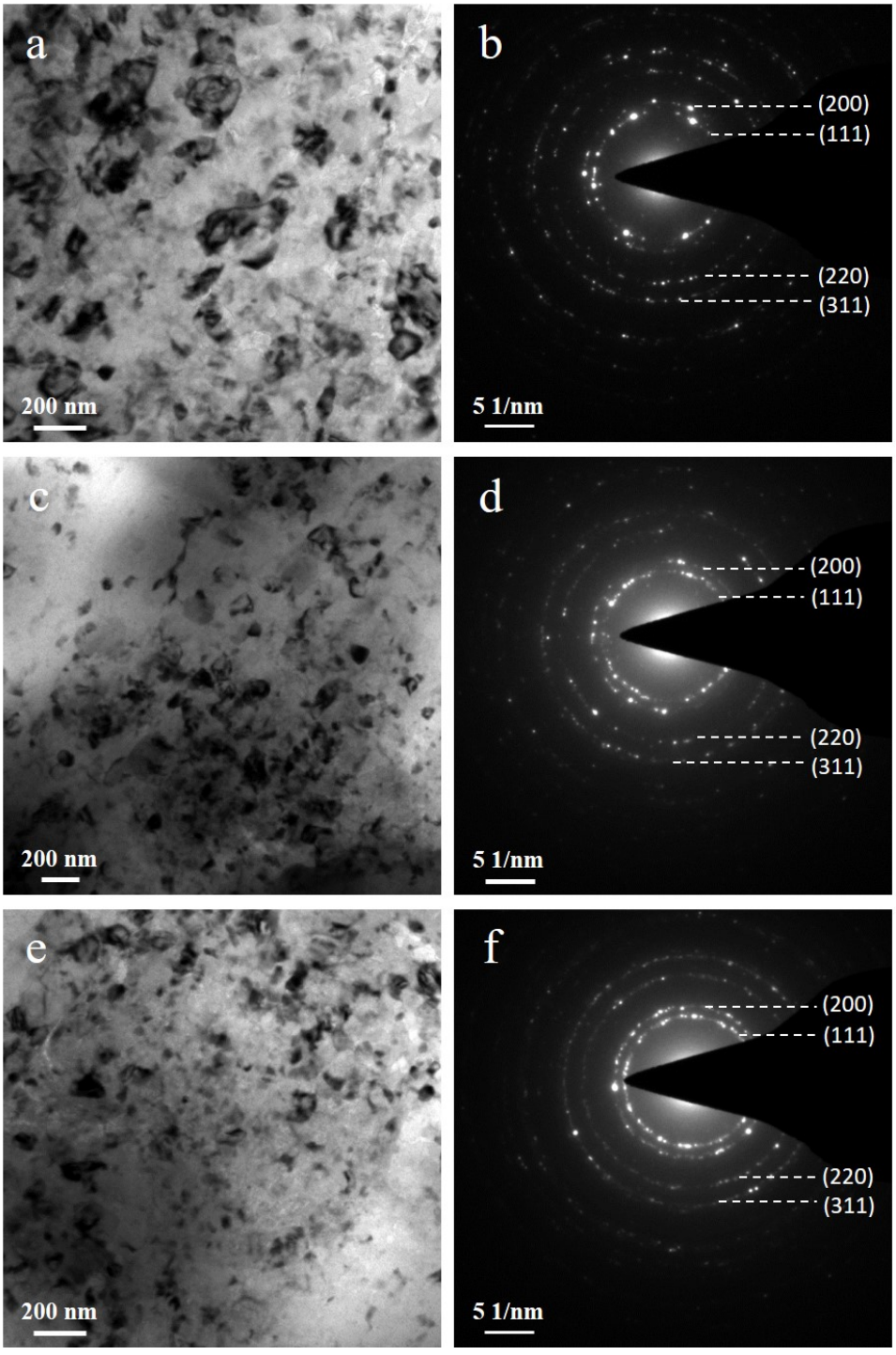
a
200 nm
b
(200)
(111)
(220)
(311)
5 1/nm
c
200 nm
d
(200)
(111)
(220)
(311)
5 1/nm
e
200 nm
f
(200)
(111)
(220)
(311)
5 1/nm

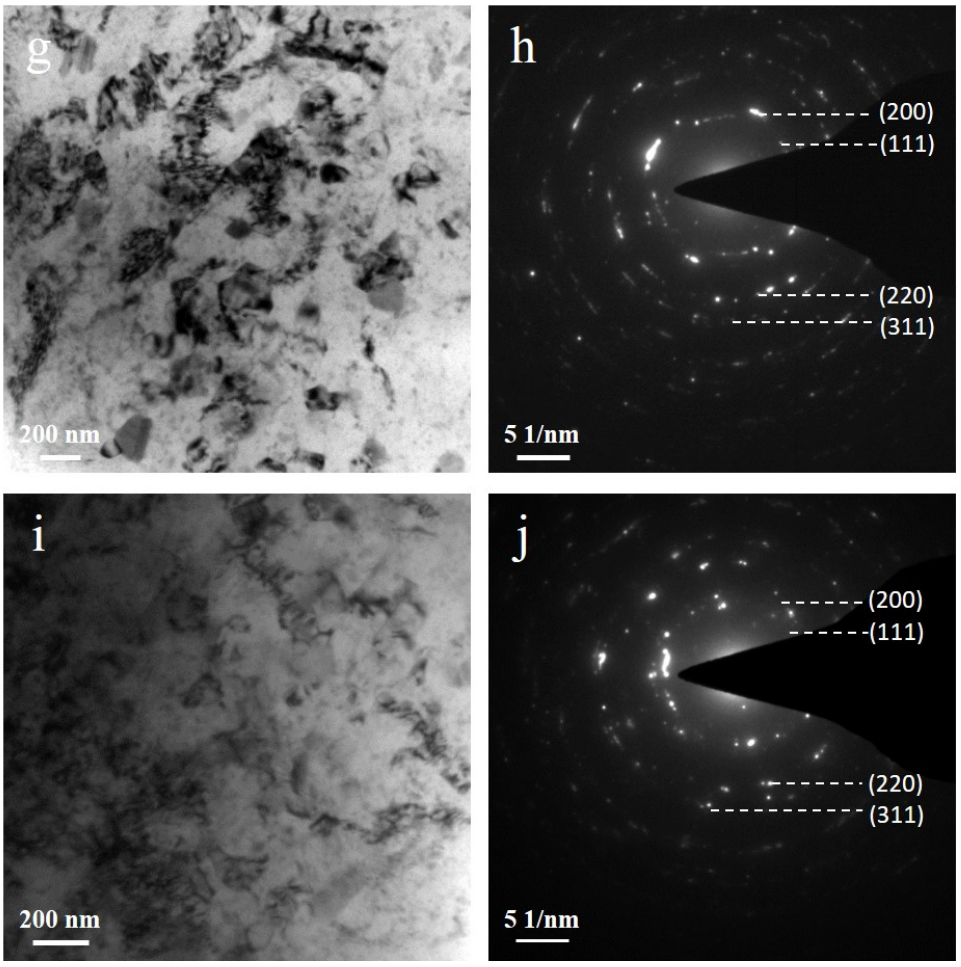

FIGURE 3.6: Bright field TEM micrographs and their corresponding SAD patterns from the top surface regions of the AA7075 in different USSP treated conditions: (a) USSP 15, (c) USSP 30, (e) USSP 60, (g) USSP 180 and (i) USSP 300.

300, it may be due to dissolution/refinement of precipitates due to the USSP treatment. High density of dislocation network and dislocation tangles may be seen inside the grains, likewise the contrast within the grains is not uniform and indicates high level of internal stresses. Second phase particles are not seen possibly due to their fragmentation to very small size and ultimate dissolution, resulting from USSP.

3.2.2.2 Microstructure evolution of USSP treated AA7075

The depth wise microstructure evolution of the gradient structured AA7075 was examined using transmission electron microscope. The top surface region of the USSP 30 specimen shows presence of nanograins (Fig. 3.7a1) and the grains are equiaxed as observed in dark field image in Fig. 3.7a2.

No precipitates were observed in the surface region possibly due to their dissolution into the matrix resulting from the severe plastic deformation caused by repeated multiple impacts of the steel balls. The corresponding SAED pattern in Fig. 3.7a3 shows continuous ring confirming the presence of nanograins with random crystallographic orientation. The average grain size in the USSP treated region was found to be 13 nm. The TEM micrograph obtained at the depth of about 2 μm is shown in Fig. 3.7b1, where the morphology of the grains is same as that of the top surface.

The microstructure consists of equiaxed grains of about 17 nm and there is no obvious change in the SAED pattern. The equiaxed nanograins were found to exist up to the depth of $\sim$ 20 μm. The bright field TEM micrograph at a depth of 12 μm is shown in Fig. 3.7c1. The morphology of the grains is elongated type as seen from the dark field image, and the discontinuity in the SAED pattern depicts coarsening of the grains (Fig. 3.7c3). A large difference in grain size can be seen suggesting presence of bi modal grain size distribution. Fig. 3.7d1 shows bright field TEM micrograph from the depth of about 47 μm below the treated surface. The grain were slightly bigger in size but still in nano regime of 43 nm. Along with the ultra fine grains there was also presence of subgrains formed by the systematic arrangement of dislocations.

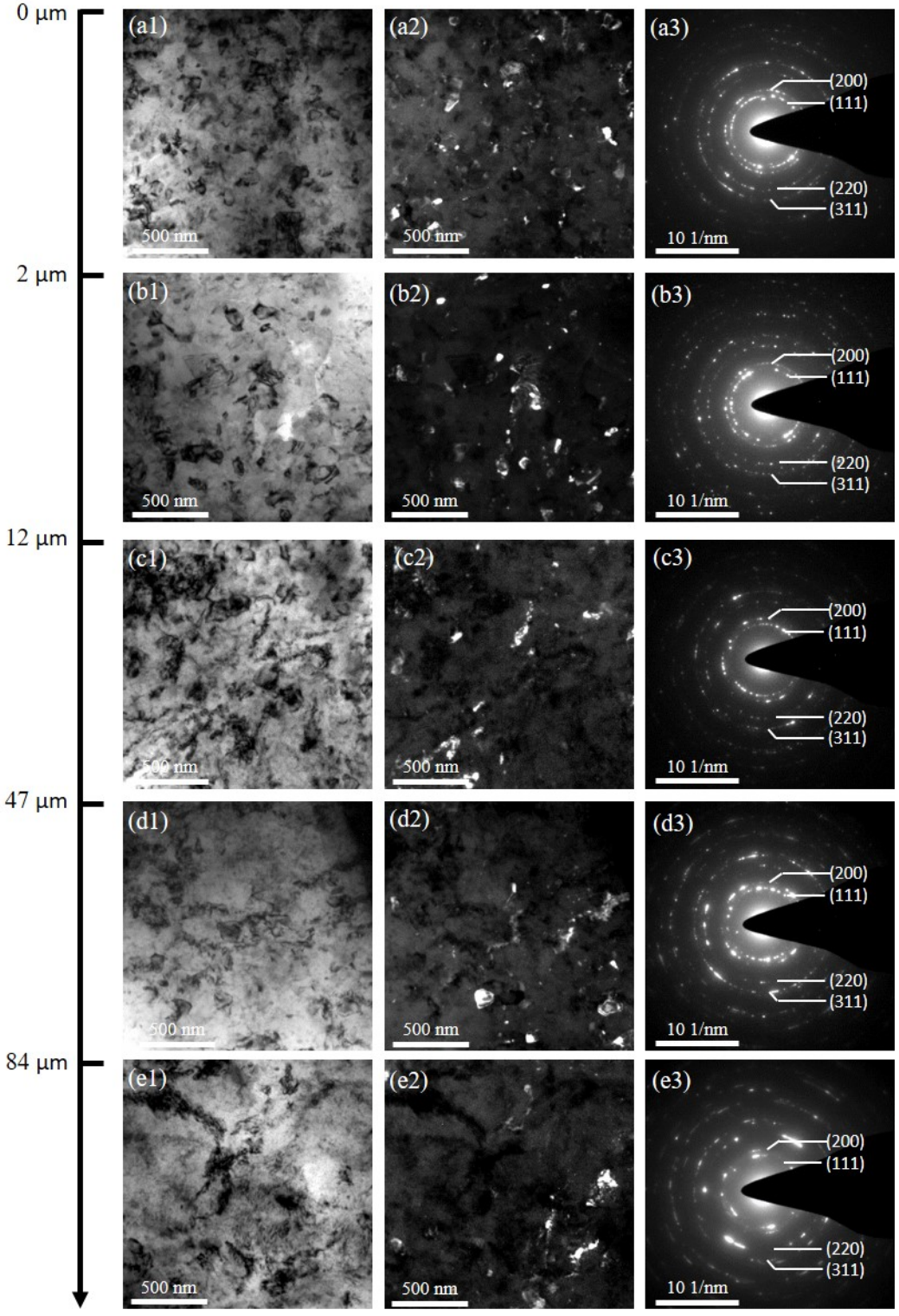

FIGURE 3.7: Bright field TEM micrographs showing microstructure evolution at different depths of the AA7075, USSP treated for 30 seconds.

At the depth of 84 μm, higher-density dislocations are found in the grain/sub-grains interior resulting from the severe plastic deformation caused by USSP treatment. The highly dense dislocations were present mostly in the tangles and there was not much effect of USSP treatment at this depth. Besides, streaking in the SAED pattern in Fig. 3.7e3 demonstrates small misorientations between the neighboring sub-grains and increase in the grains size. Presence of second phase precipitates was not observed even up to the depth of around 100 μm for the USSP 30 sample.

Microstructure evolution of the AA7075 USSP treated for 300 seconds was also investigated as a function of the depth, using TEM as shown in Fig. 3.8. The original coarse grained structure was refined to nanograins which is evident from the bright and dark field TEM micrographs in Fig. 3.8a1 and Fig. 3.8a2. The depth wise microstructure evolution revealed that it was similar to that of the USSP 30. Equiaxed nanograins were formed up to the depth of $\sim 30\mu$m as shown in Fig. 3.8c1 and equiaxed ultrafine grains were there up to the depth of 33 μm.

Elongated ultrafine grains are observed at the depth of 96 μm below the treated surface, the microstructure at the depth of 212 μm composed of dense dislocation walls and dislocation tangles and below this there was strain free matrix, unaffected by the USSP treatment. The depth of deformation was more in the sample USSP treated for higher durations. The comparison of different deformation zones for the different USSP duration was done using EBSD analysis and is presented in the following section. Based on these observations the different deformation zones in the gradient structured layer processed by USSP treatment can be chronologically distinguished from the top surface as equiaxed

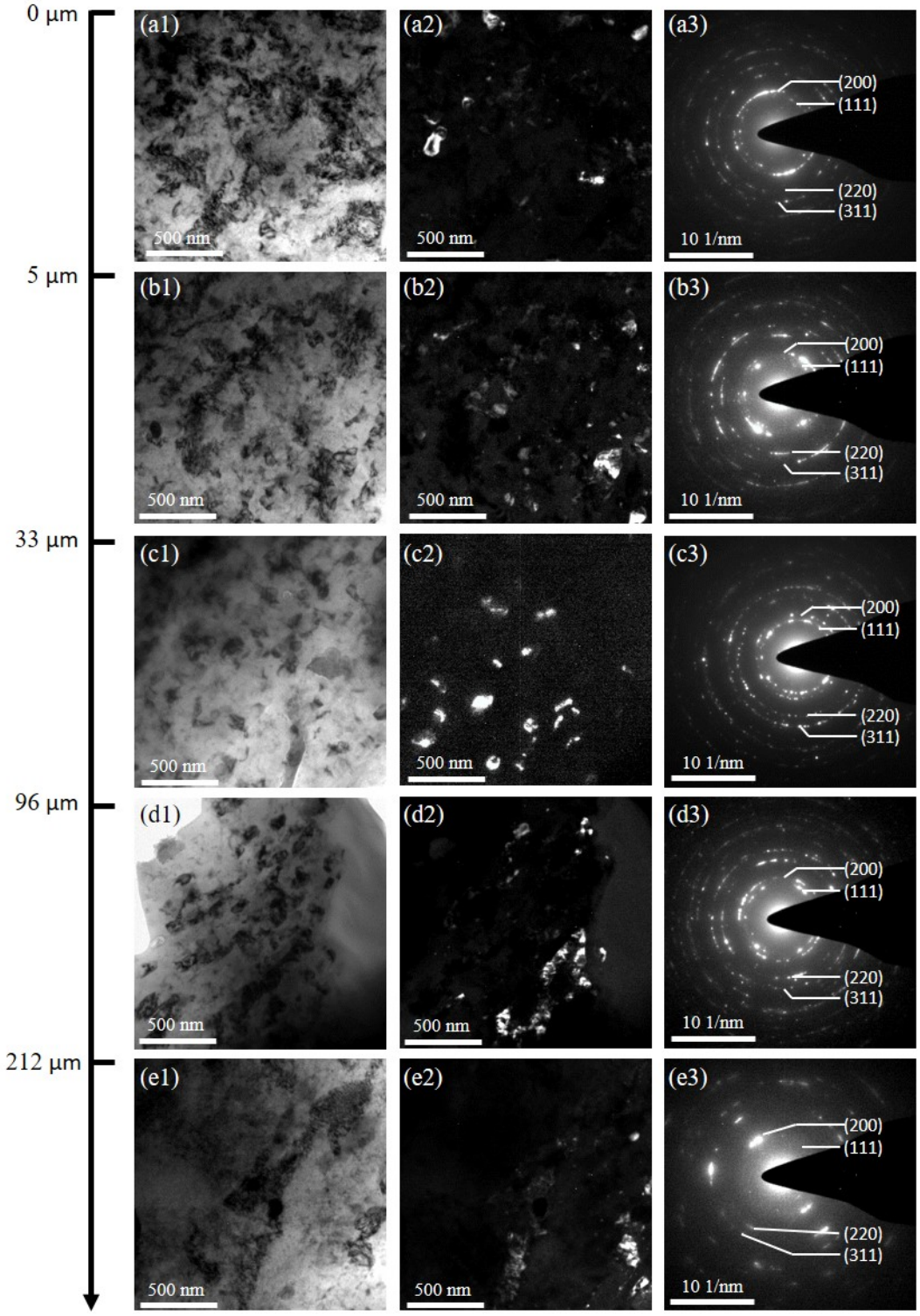

FIGURE 3.8: Bright field TEM micrographs showing microstructure evolution at different depths of the AA7075, USSP treated for 300 seconds.

nanograins, equiaxed ultrafine grains, elongated ultrafine grains and strain free matrix.

3.2.3 Electron Backscattered Diffraction (EBSD) analysis

Fig. 3.9 shows the image quality (IQ) map and Fig. 3.10 shows auto grain map of cross-section of the un-USSP, USSP 30, USSP 180 and USSP 300 samples. The un-USSP sample exhibits lamellar grain structure aligned to a particular direction. For the USSP treated specimen, dark regions (Fig. 3.9a, 3.9b, 3.9c) near the USSP treated surface correspond to heavily strained regions, giving rise to blurred or overlapped Kikuchi patterns that could not be indexed. This region corresponds to heavily deformed microstructure containing nanograins due to which the EBSD technique was unable to resolve the structure due to which the indexing rate was low. The top surface region constitutes equiaxed nanograins, revealed by TEM. The depth of this nanograined region was found to increase with increase in the duration of the USSP treatment, as shown in Fig. 3.10.

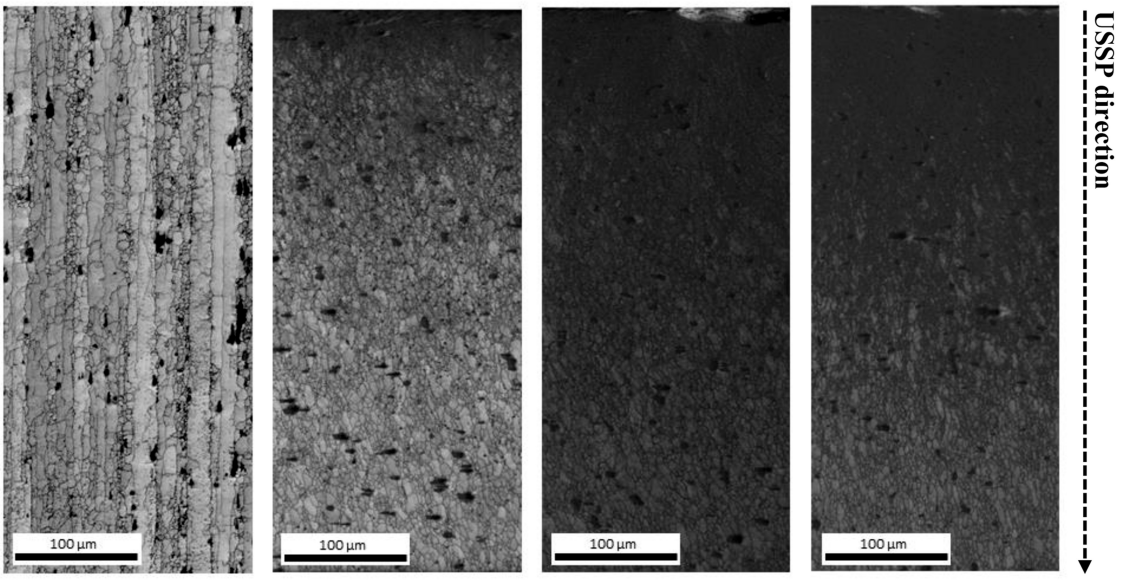

FIGURE 3.9: IQ maps of the AA7075 in different conditions (a) un-USSP, (b) USSP 30, (c) USSP 180 and (d) USSP 300.

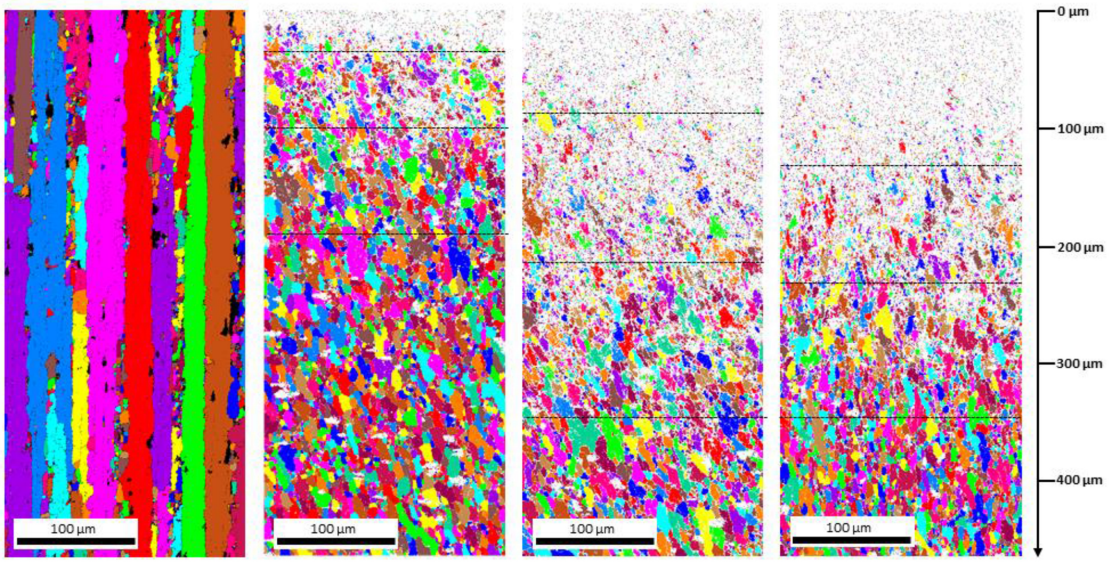

FIGURE 3.10: Auto grain maps of the AA7075 in different conditions (a) un-USSP, (b) USSP 30, (c) USSP 180 and (d) USSP 300.

As the distance from the surface increases, the indexing rate increases and the EBSD technique starts recording fine domains that clearly originate from the grain and sub-grain divisions. The microstructure varies in a graded manner from the top treated region towards interior. As the depth from the top surface increases, the grain size gradually increases. Below the nanograined region there are equiaxed ultrafine (>100 nm) grains. Further, presence of elongated ultrafine grains is observed, however, beyond this it contains strained grain structure. The total depth of the different deformation regions for the different USSP conditions is shown in Fig. 3.11. It is clear that the depth of deformation increases with increase in the USSP treatment time but gets saturated after a particular duration. For USSP 300 the depth of nanostructured layer is relatively large as compared with that of USSP 180, however the total depth of the deformed region is almost comparable ($\sim$ 350 μm).

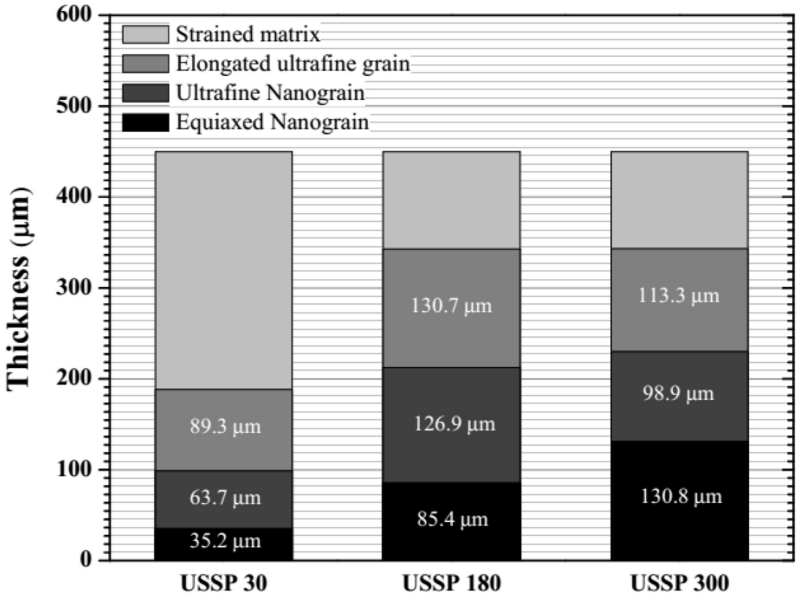

FIGURE 3.11: Thickness of the different types of microstructure layers.

The misorientation within the microstructure is shown by the grain boundary misorientation map in Fig. 3.12. Red colored grain boundaries correspond to low angle misorientation ($<15°$), whereas black colored grain boundaries depict high angle misorientation ($>15°$).

In the un-USSP condition low angle boundaries constitute major fraction (0.672). USSP treatment generates grain boundaries with high angle misorientation and this misorientation increases with increase in the USSP duration and this misorientation also tends to saturate with increase in the deformation. The variation of grain boundary misorientation for different conditions is shown in Fig. 3.13. Information obtained from EBSD analyses was used to provide an insight of the microstructure evolution resulting from USSP treatment. In particular, the thickness of the different deformation zones usually

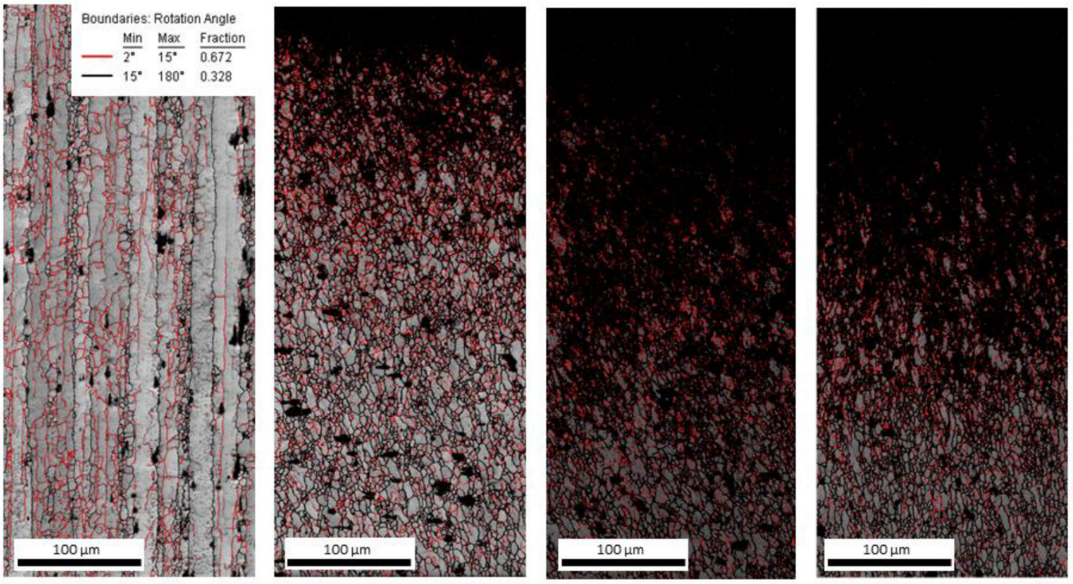

FIGURE 3.12: Grain boundary misorientation maps of the AA7075 in different conditions (a) un-USSP, (b) USSP 30, (c) USSP 180 and (d) USSP 300.

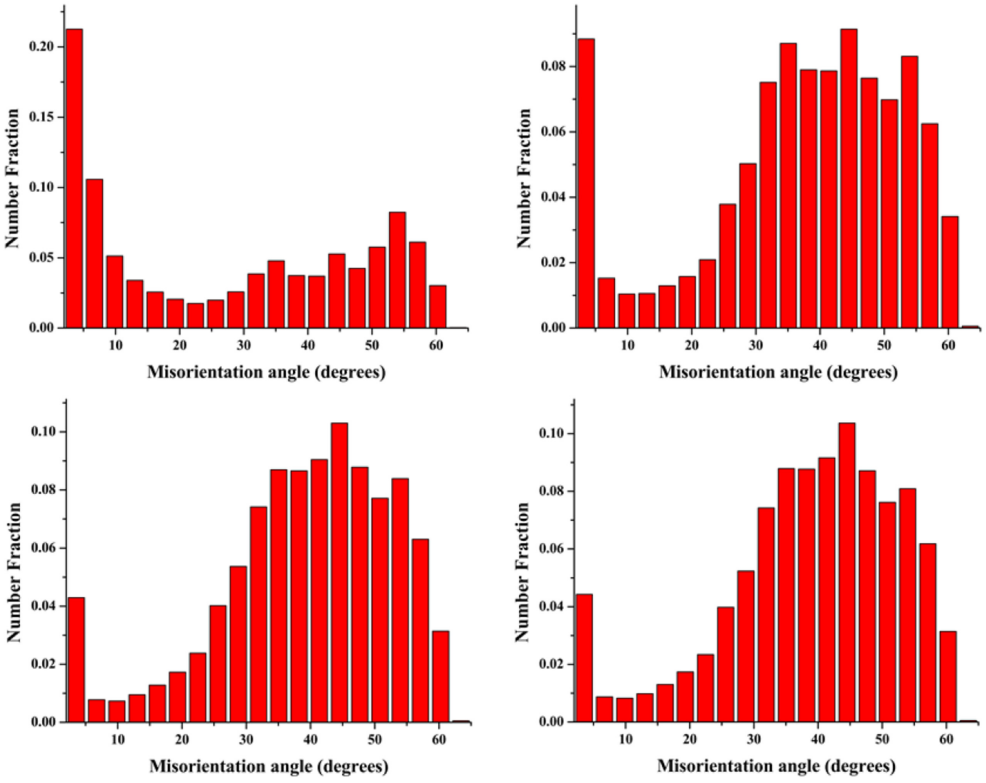

FIGURE 3.13: Variation of grain boundary misorientation of the AA7075 in different conditions (a) un-USSP, (b) USSP 30, (c) USSP 180 and (d) USSP 300.

depicted in the USSP treated samples are: (i) nanostructured region having largely nano-sized grains that correspond to the ultimate stage of grain refinement under heavy deformation, (ii) transition zone corresponding to ultrafine nanograins and ultrafine elongated grains and (iii) the strained zone where the initial grains are simply plastically deformed.

3.3 XRD Analysis of USSP Treated AA7074

XRD patterns of the specimens subjected to different durations of USSP are shown in Fig. 3.14 and there are only aluminium peaks in all the cases including the USSP 300. The magnified view of the (311) peak shows that Bragg diffraction peaks of the USSP treated specimens are broader than that of the un-USSP one and the extent of broadening increases with the duration of USSP. The shift in the diffraction angle towards lower side of the angle is also evident. Broadening of the diffraction peaks could be due to grain refinement whereas the shift of the peak may be attributed to increase in the atomic level lattice strain caused by USSP.

The average crystallite size was calculated from the five Bragg reflection peaks of fcc-Al: (111), (200), (220), (311) and (222) using the Scherrer and Wilson equation [81].

$$t = \frac{0.9\lambda}{Bcos\theta} \tag{3.1}$$

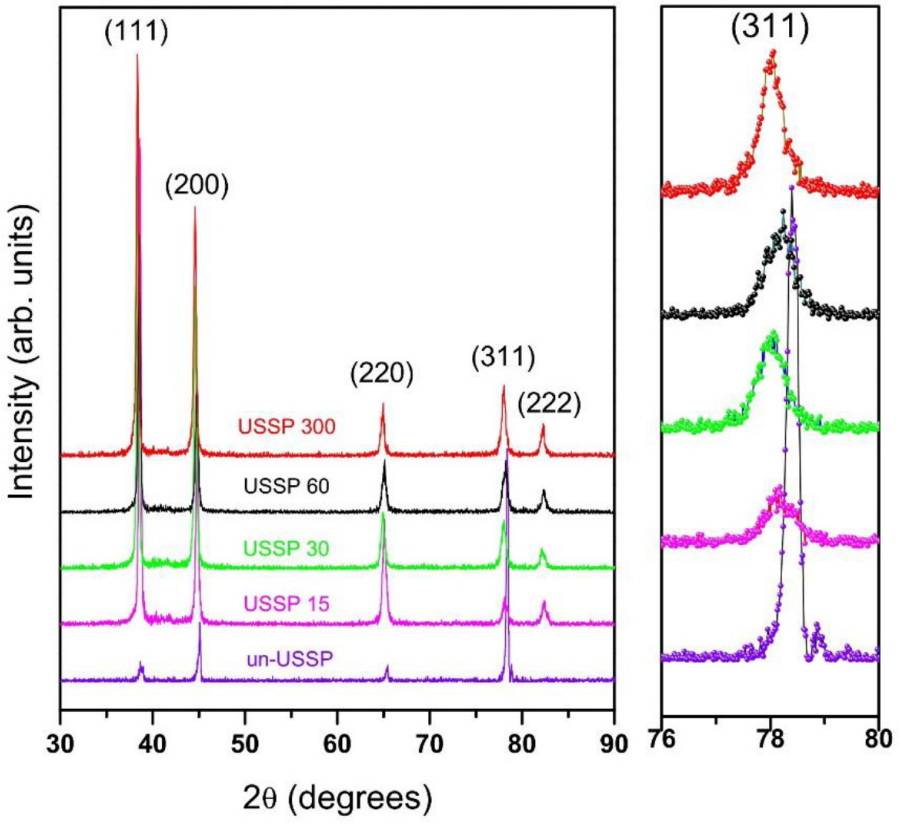

FIGURE 3.14: XRD patterns of the 7075 Al alloy in the un-USSP condition and USSP treated for different durations of time.

Where t is the effective crystallite size, λ is X-ray wavelength, θ is Bragg angle and B is line broadening. The micro-strain was calculated using the Williamson Hall equation [82].

$$Bcos\theta = [\frac{0.9\lambda}{t}] + [4\varepsilon sin\theta] \tag{3.2}$$

Where ε is root mean square of micro-strain.

The average crystallite size and mean micro-strain as a function of USSP time are shown in Fig. 3.15a. The average crystallite size decreased from 21 nm to 16 nm with increase in the treatment time from 15 to 300 seconds and there was substantial increase

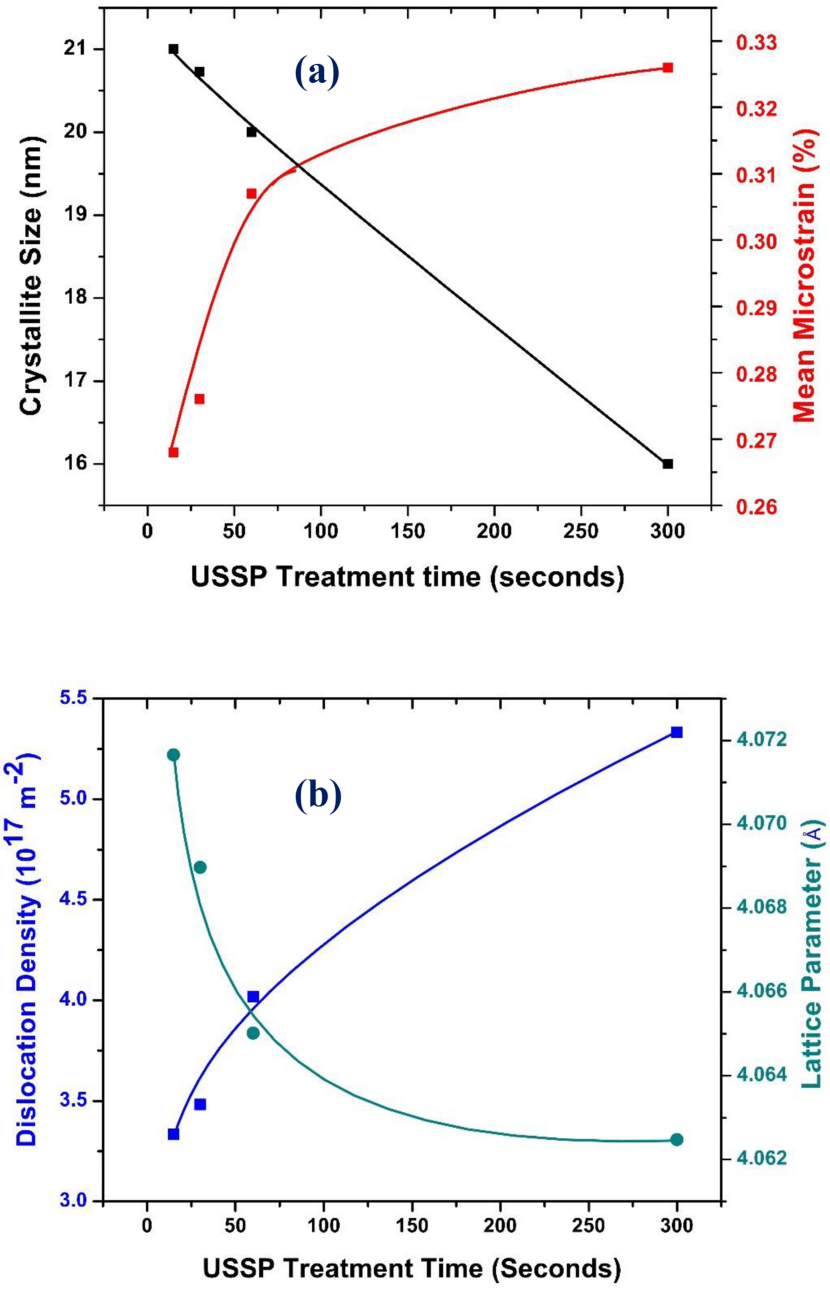

FIGURE 3.15: (a) Variation of average crystallite size and mean micro-strain and (b) Variation of dislocation density and lattice parameter with treatment time of USSP in the AA7075.

in the micro-strain with increase in the treatment time. The dislocation density was calculated using the relationship given below [83].

$$\rho = \frac{3\sqrt{2\pi} < \varepsilon^2 >^{1/2}}{Db} \tag{3.3}$$

Where ε is micro-strain, D is average crystallite size, b is burgers vector (b=$\frac{a}{\sqrt{2}}$ for FCC structure) and a is lattice parameter. The lattice parameter may be seen to decrease from approximately 4.072 to 4.062 with increase in the USSP duration (Fig. 3.15b).

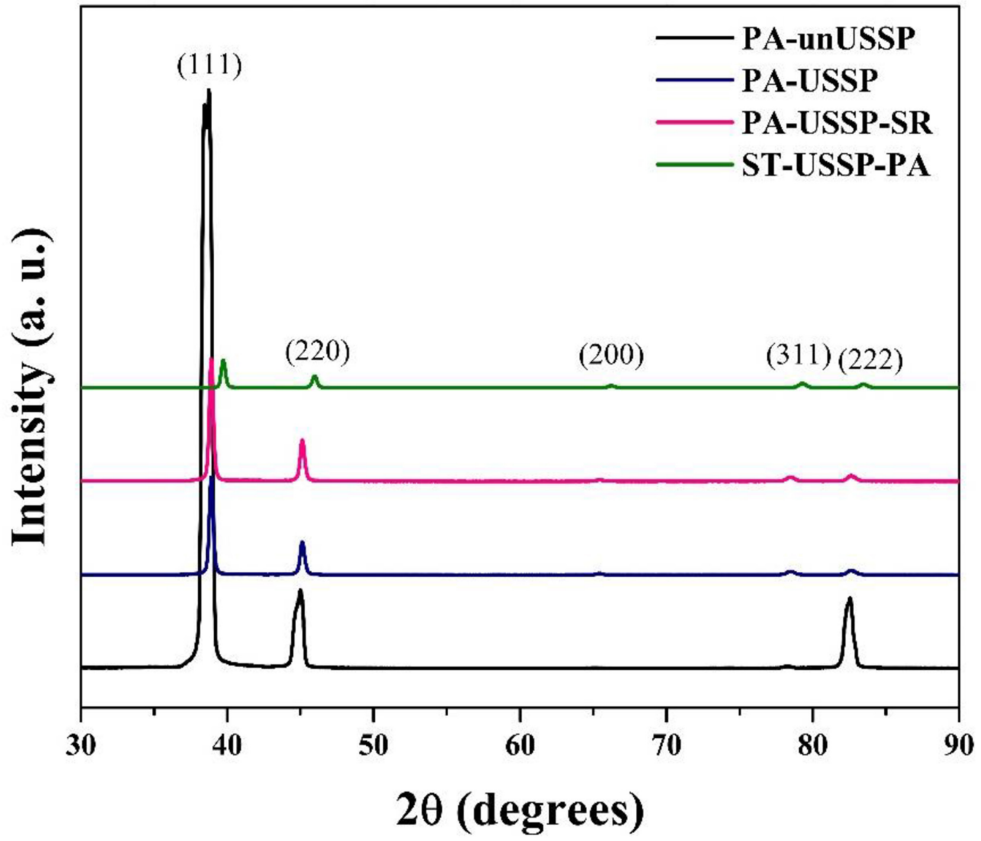

FIGURE 3.16: XRD patterns of the AA7075 in different conditions.

Also, dislocation density was increased with increase in the USSP duration due to generation of dislocations from continuous impact of balls (Fig. 3.15b).

X-ray diffractographs of the AA7075 in the PA-unUSSP, PA-USSP (180 seconds),

PA-USSP-SR (peak aging followed by USSP treatment then stress relieving) and ST-USSP-PA (solution treated followed by USSP treatment and peak aging) samples are shown in Fig. 3.16. XRD was done to see whether there was any phase transformation resulting from the heat treatment. As seen from Fig. 3.16, there are peaks exclusively of α -aluminium in all the conditions; thus, it is obvious that there was no phase transformation due to the different thermal treatments. The average crystallite size in surface region of the PA-USSP, PA-USSP-SR and ST-USSP-PA was 19 nm, 22 nm and 21 nm, respectively. Thus, there was retention of the nanostructure in surface region of the specimens in all the above conditions. Microstrain for the PA-USSP, PA-USSP-SR and ST-USSP-PA conditions was found to be 0.320, 0.307 and 0.304% respectively.

3.4 Residual Stress Distribution

The variation of residual stress of the different USSP treated specimens along the depth from the USSP treated surface is shown in Fig. 3.17. The residual stress is compressive in nature and is maximum at the sub-surface. It increased with the duration of USSP. For the USSP 300 sample the residual stress was -265 MPa at the surface, increased to maximum level of -410 MPa at the depth of 10 μm and decreased to $\sim$ -200 MPa at the depth of 250 μm. On the other hand it was almost zero for the USSP 15 at the depth of 250 μm.

The variation of residual stress for different heat treated samples was also measured (Fig. 3.18). Here, also the residual stresses shows that they were compressive in nature and maximum in the sub-surface region. The maximum compressive residual stress was -305 MPa for the PA-USSP. The magnitude of the compressive stress was reduced to 239

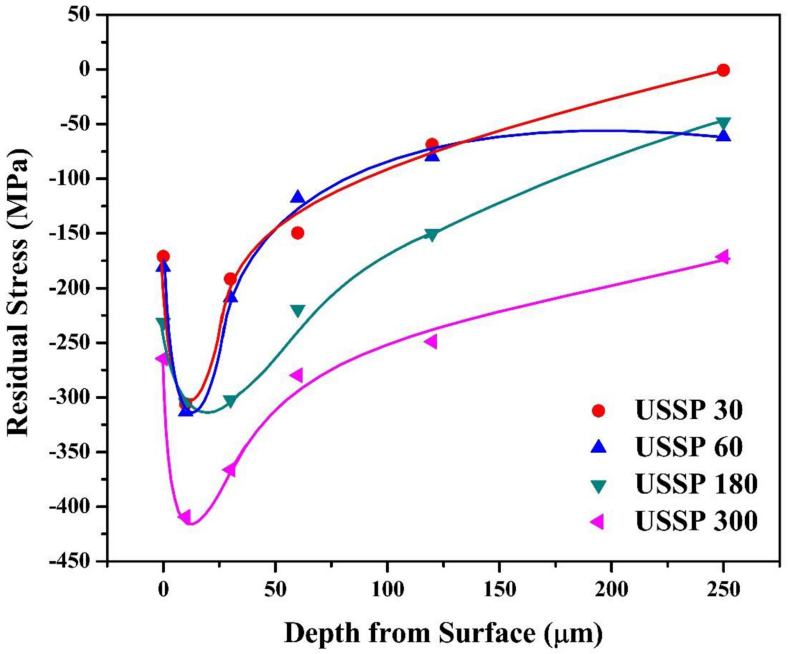

FIGURE 3.17: Variation of the residual stress along the depth from the surface of the AA7075, USSP treated for different durations.

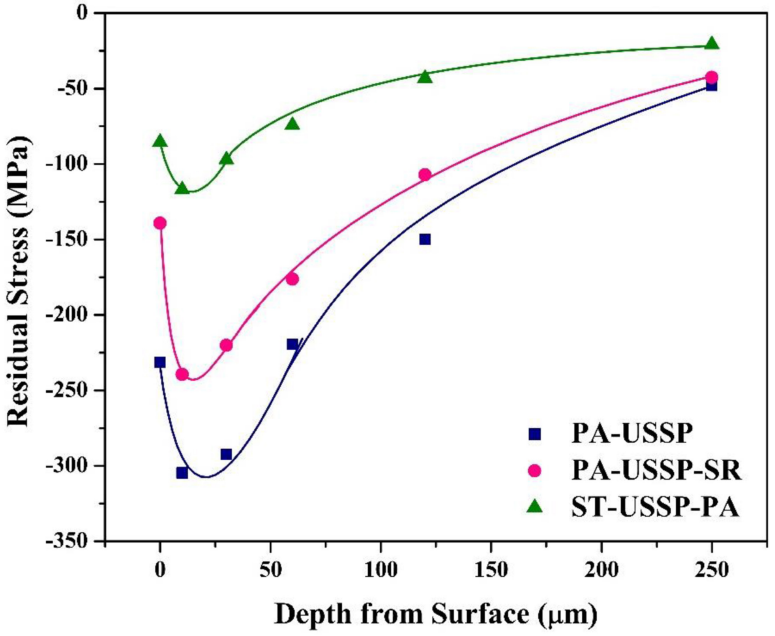

FIGURE 3.18: Distribution of residual stress in the AA7075 in different conditions.

MPa and 117 MPa for the PA-USSP-SR and ST-USSP-PA respectively. It is evident from the profile of the stress distribution that the major compressive stress was relieved from thermal exposure of the samples at higher temperatures, up to the depth of $\sim$ 250 μm and the nature of the residual stress was still compressive.

3.5 Surface Roughness Variation

The variation of average surface roughness (R_a) of the un-USSP sample and those USSP treated for different durations is shown in Fig. 3.19. It may be seen that the un-USSP surface is much smoother than the USSP treated ones. While R_a of the un-USSP sample is 0.23 μm, it progressively increased with the duration of USSP and reached to 4.08 μm for the USSP 300 sample.

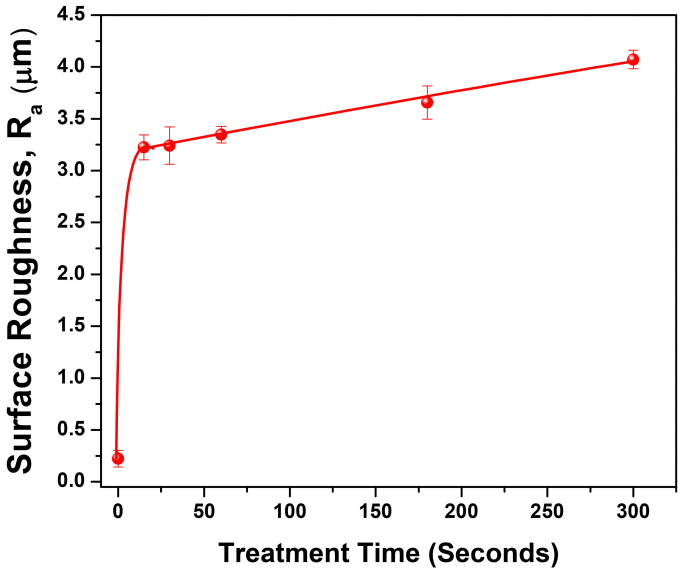

FIGURE 3.19: Variation of average surface roughness of the AA7075 with duration of USSP.

3.6 Microhardness Variation

The microhardness profiles of transverse sections of the USSP treated specimens in Fig. 3.20 show variation of microhardness from surface of the USSP treated specimen towards the interior. The hardness is maximum in the surface region and gradually decreases towards the substrate.

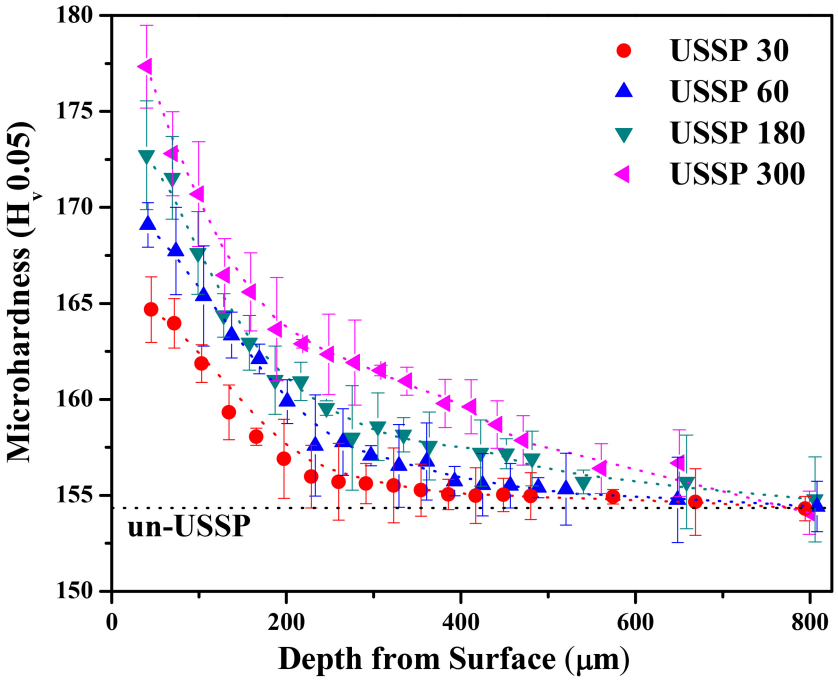

FIGURE 3.20: Variation of microhardness from the surface towards interior of the AA7075, USSP treated for different durations.

The gradual decrease in the hardness is due to the gradient microstructure resulting from the USSP treatment. Microhardness of the surface region and also the depth of the affected region increased with the duration of the treatment. The hardness of the un-USSP treated sample was 154 H_v and it increased to 177 H_v for the USSP 300 sample.

The variation of microhardness from the USSP treated surface towards interior in transverse sections of the different heat treated sample is shown in Fig. 3.21. The hardness was highest in the surface region and gradually decreased with increase in the depth from the surface. The hardness of the PA-unUSSP sample was 154 H_v which increased to 173 H_v in the surface region following the USSP treatment. The high hardness of surface region of the USSP treated specimen was reduced to 168 H_v following stress relieving treatment at 90°C for 4 hours. The microhardness of the ST-USSP-PA was 185 H_v.

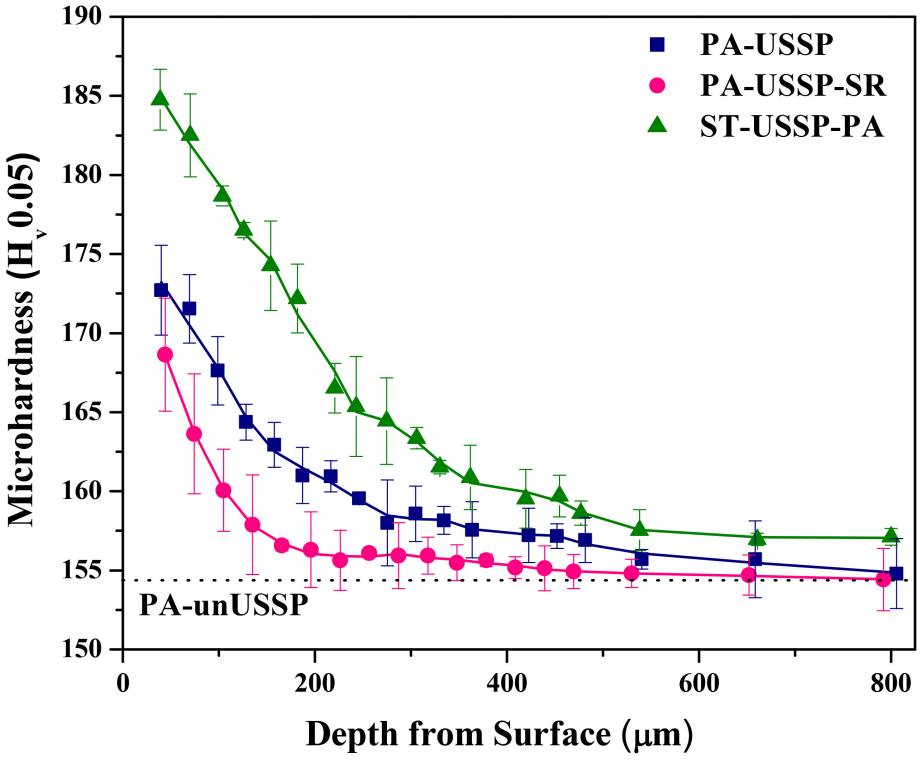

FIGURE 3.21: Variation of microhardness of the AA7075 in the different conditions.

3.7 Discussion

Based on TEM and X-ray diffraction results it was confirmed that there was formation of a nanocrystalline layer near the treated surface. The original coarse grained structure was refined to nano-scale and it was due to the severe plastic deformation caused by the repeated multi directional impact of hard steel balls. Plastic deformation causes strain gradient in the cross-sectional area of the treated specimen which yields dislocations in the alloys having high density near the surface region. In order to accommodate further straining these dislocations rearrange themselves causing dislocation gliding, accumulation, tangling and interaction [84, 85].

As seen from Fig. 3.6 there was formation of nanograins in the samples USSP treated for the duration of 15, 30, 60, 180 and 300 seconds respectively. There was also formation of large number of dislocation tangles which ultimately resulted in refinement of the microstructure in near surface region. The mechanism of grain refinement of materials with high stacking fault energy has been reported to be associated with deformation by dislocation slip. The observation of nanostructuring in the present investigation is in line with the proposed mechanism of formation of dislocation tangles in FCC system resulting at high strain rates near the surface region [86]. Wu et. al [39] observed the microstructural evolution of USSP treated 7075 aluminum alloy at different depths from the top treated surface. They observed that a layer of 62 μm thick ultrafine grains was introduced into the surface layer. In the top region of high strain there was formation of equiaxed nanograins with high misorientation, below that equiaxed sub-micro grains were observed. Parallel microband with elongated grains were formed at low strains near the original unaffected

matrix.

The sub-division of the grains does not continue indefinitely with USSP duration, it gets saturated after some time and further straining does not affect the microstructure. The random bombardment of balls in USSP provides multiple strain paths and high strain rate which lead to sub grain rotation. Subgrain rotation is the primary mechanism for accommodation of large deformation. With increase in strain the subgrains do not undergo plastic deformation by slip and begin to rotate. This results in highly misoriented equiaxed microstructure.

The XRD pattern of un-USSP and different USSP treated specimens is shown in Fig. 3.14. It was observed that the diffraction peaks of the USSP treated samples got broadened with increase in the treatment duration. The broadening of the peak is mainly due to the combined effect of grain refinement, microstrain and instrumental broadening. Here broadening of the peak may be attributed to grain refinement and increase in the microstrain. Quantitative analysis of the XRD plots also confirmed refinement of the surface microstructure to nano level.

It is known that the strain rate decreases with increase in depth from the top surface treated by USSP [39]. Various dislocation activities are normally activated, including slip, accumulation, interaction, tangling, and spatial rearrangement in order to accommodate plastic strains. In this way, Fig. 3.22 represents the physical mechanisms of the grain refinement of AA7075 treated with USSP. Based on the microstructural features observed in various layers with different strains, the following states are involved in the process of grain refinement:

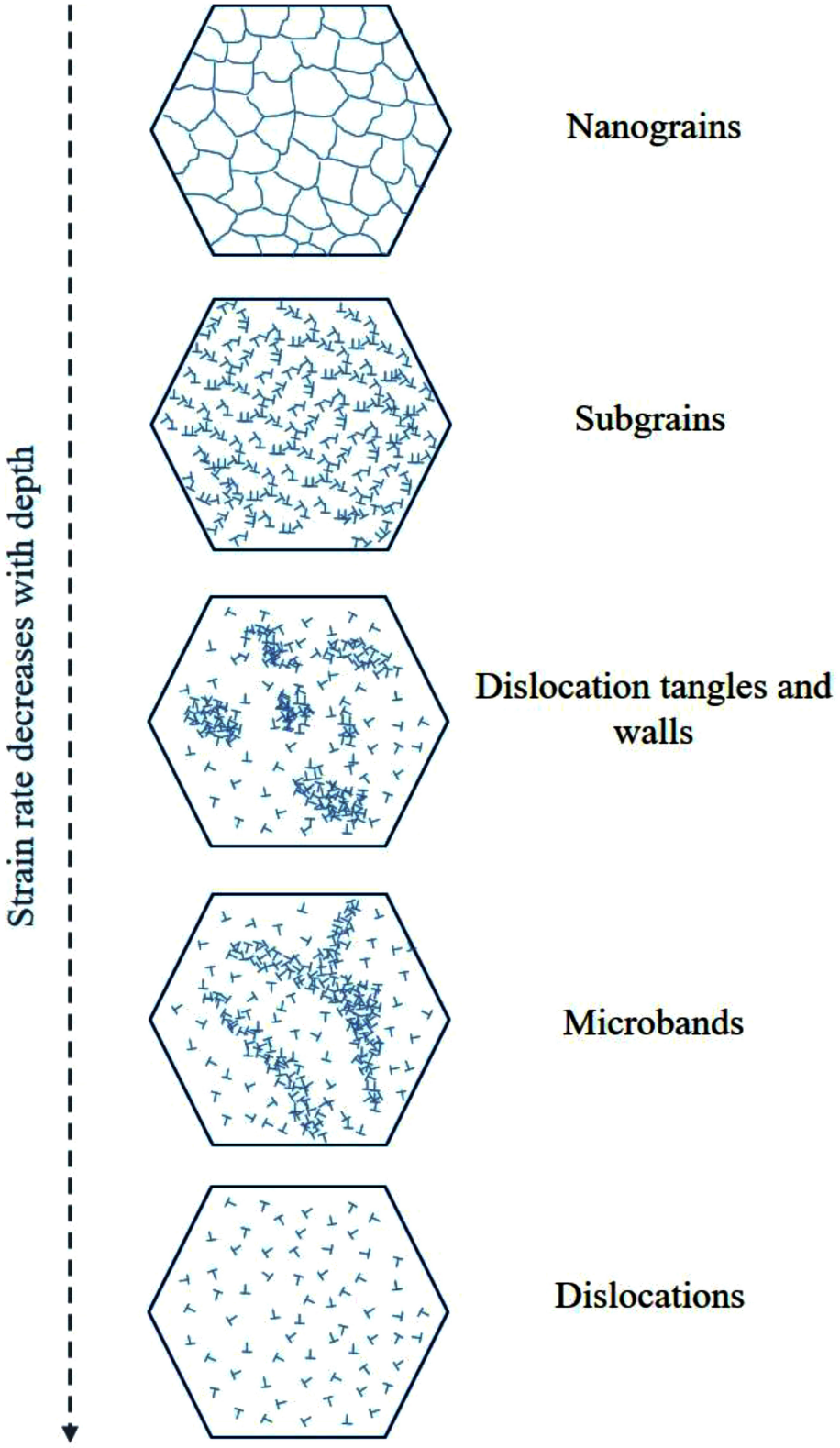

FIGURE 3.22: Schematic illustration showing microstructural evolution process of the AA7075 treated with USSP.

i. Development of dislocation within the grains.

ii. With continuous increase in strain, the density and interaction of dislocations are increased resulting in formation of dislocation cells arranged in the form of microbands.

iii. Increase of plastic strain results in accumulation of dislocations and produces structures in the form of dislocation tangles and dislocation walls due to the pile up of the dislocations.

iv. With further increase in strains the total energy of original grain is minimized by dislocation annihilation resulting in the sub-division of original coarse grains into sub-grains.

v. In the region of high strains formation of nanograins results due to the progressive accumulation of boundary misorientation, and finally leading to a gradual transition of boundaries character until the formation of high angle grain boundaries occurs.

A gradient structure develops after the USSP treatment as observed by the depth dependent microstructural evolution from TEM and EBSD studies. As depth from the top most surface decreases, the grain size was found to reduce. During the early deformation, at lower depth the generated dislocations interact with each other to produce various configurations. In order to minimize the total free energy dislocation cells are formed and are repeatedly divided into finer cells on further straining. Higher rate can even lead to direct formation of microbands. In the region with higher strain rate near the surface region finer grains are observed with grain rotation thus misorientation in nanograins increases. Therefore, increasing strain rate effectively reduces the structural scale. Second-phase particles also significantly affect the deformation behavior, simultaneously improving strength and

ductility of the nanostructured materials [87, 88].

Apps et. al [89] reported that the rate of dislocation generation increases by $\sim$ 10 times in Al–0.2Sc alloy with Al_3Sc dispersoids at low strains as compared to pure metals. The rate of dislocation multiplication is associated with the relationship between the matrix and particles, and particle features such as particle size, inter-particle spacing, and particle volume fraction. At low strains, T-phase particles promote dislocation generation by acting as emission source [39] or as a barrier [90] which leads to accumulation of dislocations; however, areas without T-phase particles exhibit limited dislocations. Grain boundary strengthening and dislocation strengthening induced by SPD led to a significant increase in strength of pure metals, but limited increase for the age-hardened alloys. This is one of the main sources of strength improvement of the gradient structured samples with increasing thickness [91]. Apart from the evidence of obtaining finer grains around second phase particles, strain gradient also promotes the operation of additional slip systems and increases the dislocation storage in nanograins [92]. Therefore, for the nanostructured materials, the dislocation-dominated properties, such as, ductility, are expected to improve by methods involving increasing strain rate [93] and strain gradient [94].

The microhardness near the surface region was found to be relatively higher and increasing with increase in the USSP treatment duration (Fig. 3.20). Grain refinement, increase in dislocation density and high compressive residual stress near the surface region resulted in increase of the surface hardness. The microhardness decreased from surface towards the interior and was due to gradient microstructure having nanograins in the surface region followed by sub-micron grains and the the original coarse grains at a particular

depth. The depth of the severely plastically deformed layer increased with increase in the USSP treatment duration. Many investigations have shown that the reduction in grain size results in increase in hardness [95, 96]. According to the Hall-Petch relationship, the hardness of a material increases with decrease in grain size. In addition, work hardening caused by the process of USSP, has also some contribution to the improvement of hardness. Hence, the increase of hardness for the USSP treated sample can be attributed to refinement of grains and work hardening.

It may be seen from Fig. 3.19 that there is marked increase in the average surface roughness of the USSP 15 sample. Further increase in the USSP duration leads to very marginal increase in the surface roughness [97–99]. The nature of variation of the roughness with duration of USSP may be understood in terms of the opposite processes controlling the roughness. Initially, the roughness increases significantly due to rapid increase in height of the ridges resulting from the indentations created by shots. However, during the longer periods of USSP the process of abrasion starts because of excessive work hardening of the surface region, resulting in a marginal increase in the surface roughness. The effect of the two opposite processes appears to be comparable during USSP from 15 to 30 second to cause little change in the roughness. However, with increase in USSP from 30 to 60 second there is nominal increase in roughness from chipping as evident from Fig. 3.2d. Further increase in the duration of USSP to 300 sec leads to considerable increase in the surface roughness which is attributed to flaking and cracking at the surface (Fig. 3.3c).

3.8 Conclusions

The following conclusions are drawn from this chapter:

1. Nanostructure of 19-28 nm size developed in surface region of the AA7075 from USSP for different durations.

2. The different deformation zones in gradient structured layer can be distinguished from the top surface as equiaxed nanograins, equiaxed ultrafine grains, elongated ultrafine grains and strain free matrix.

3. The total depth of deformed region was found to increase with increase in USSP duration.

4. There was no phase transformation in the alloy due to USSP even after the longest USSP duration of 300 s.

5. Microhardness was maximum in the surface region and was gradually reduced from surface towards the interior.

6. Maximum compressive residual stress developed at the depth of ~ 10 μm from the treated surface.

7. Surface roughness was found to increase with increase in the USSP duration.